Martínez-Haya, R.; Heredia, AA.; Castro-Godoy, WD.; Schmidt, LC.; Marín García, ML.; Argüello, JE. (2021). Mechanistic Insight into the Light-Triggered CuAAC Reaction: Does Any of the Photocatalyst Go?. Journal of Organic Chemistry. 86(8):5832-5844. https://doi.org/10.1021/acs.joc.1c00272

Mechanistic Insight into the Light-Triggered CuAAC Reaction, does any Photocatalyst go?

Rebeca Martínez-Haya,[a] Adrián A. Heredia,[b] Willber D. Castro-Godoy,[c] Luciana C. Schmidt,[b] M. Luisa Marin*[a] and Juan E. Argüello*[b]

[a]Instituto de Tecnología Química, Universitat Politècnica de València-Consejo Superior de Investigaciones Científicas, Avenida de los Naranjos s/n, 46022 Valencia, Spain.
**marmarin@qim.upv.es*
[b] INFIQC-CONICET-UNC, Dpto. de Química Orgánica, Facultad de Ciencias Químicas, Universidad Nacional de Córdoba, Ciudad Universitaria, X5000HUA Córdoba, Argentina.
**jea@fcq.unc.edu.ar*
[c] Departamento de Química, Física y Matemática, Facultad de Química y Farmacia, Universidad de El Salvador, Final Av. de Mártires y Héroes del 30 de Julio, San Salvador 1101, El Salvador.

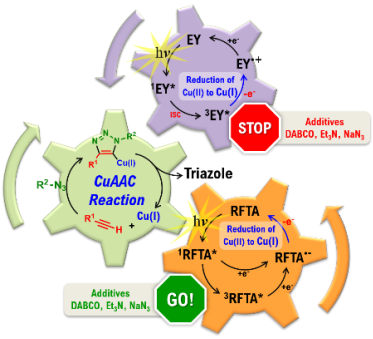

Abstract graphic

1. Abstract:

The attainment of transition-metal catalysis and photoredox catalysis has represented a great challenge over the last years. Herein, we have been able to merge both catalytic processes into what we have called 'the light-triggered CuAAC reaction'. Particularly, the CuAAC reaction reveals opposite outcomes depending on the nature of the photocatalyst (Eosin Y disodium salt and Riboflavin tetraacetate) and additives (DABCO, Et_3N, and NaN_3) employed. To get a better insight into the operating

processes, steady-state, time-resolved emission, and laser flash photolysis experiments have been performed to determine reactivity and kinetic data. These results, in agreement with thermodynamic estimations based on reported data, support the proposed mechanisms. While for Eosin Y (EY), Cu(II) was reduced by its triplet excited state; for Riboflavin tetraacetate (RFTA), mainly triplet excited RFTA state photo-reduction by electron donors as additives are mandatory, affording $RFTA^{\bullet -}$ (from DABCO and NaN_3) or $RFTAH^{\bullet}$ (from Et_3N). Subsequently, these species are responsible for the reduction of Cu(II). For both photocatalysts, photo-generated Cu(I) finally renders 1,2,3-triazole as the final product. The determined kinetic rate constants allowed postulating plausible mechanisms in both cases, bringing to light the importance of kinetic studies to achieve a strong understanding of photoredox processes.

2. Introduction

Since the beginning of the 21st century, organic chemistry has witnessed a relevant increase in research in the field of visible-light photocatalysis. Certainly, the use of visible light as a green "activator" combined with catalysts is attractive to develop effective and greener chemical transformations.[1] Thus, the photochemical approach represents an environmentally benign protocol that leads to a great diversity of molecules, unreachable through other synthetic methods.[2]

For instance, the development of new routes to synthesize 1,2,3-triazoles is an area of research of renewed interest not only due to their exceptional biological and binding properties, but also for their potential in medicinal and material chemistry applications.[3] Currently, the copper-catalyzed azide-alkyne cycloaddition (CuAAC) is the most commonly used method to synthesize 1,2,3-triazoles.[4] This reaction was developed by Sharpless and Meldal, and between the two possible produced isomers, only the

presence of Cu(I) afforded exclusively the 1,4-disubstituted regioisomer.[5] Although several copper sources can be used in the CuAAC, the formation in situ of Cu(I) at the expense of Cu (II) appears as the simplest method. Since then, the use of Cu-catalyzed methodologies is increasingly growing mainly because Cu is abundant on the earth-crust, and therefore inexpensive when compared with other transition metals like Pd, Pt, Rh, Ru, Ir, or Au.

More interestingly, there are widely developed methodologies where Cu(I) is generated *in situ* by the photoinduced reduction of Cu(II).[6] Hence, the use of light to eventually generate Cu(I) from Cu(II) expands the potential of CuAAC to the synthesis of materials in which spatial and temporal control is needed.[7] More specifically, several examples use light to reduce Cu(II) directly from complexes,[8] while others involve the use of expensive photocatalysts based on transition metals,[9] or cheaper visible-light absorbing organic photocatalysts.[10] In fact, organic photocatalysts have already demonstrated their potential in organic synthesis in a variety of photoredox processes, due to their strong visible light absorption capacity, suitable redox potentials, long-enough excited states and reasonable photostability.[11]

In photocatalyzed processes, evaluating the kinetics of excited states is crucial to postulate a plausible mechanism.[11-12] However, little attention has been paid to the exploration of the mechanism behind the light-triggered CuAAC. Only in few cases the fundamental aspects and molecular bases of such mechanism have been investigated through kinetics and spectroscopic methods, namely: laser flash photolysis (LFP),[13] Fourier-transform infrared spectroscopy (FTIR),[14] electron paramagnetic resonance (EPR),[13b,15] or single molecule spectroscopy.[16]

Herein, we report on a systematic evaluation of the role of all the species potentially involved in a light-triggered CuAAC by Eosin Y disodium salt (EY) and Riboflavin

tetraacetate (RFTA). EY is a widespread employed organic photocatalyst able to participate in oxidative and reductive cycles,[10d,12b,13b] while RFTA is more likely involved in a reductive cycle.[17] The well-known cycloaddition between benzyl azide and phenyl acetylene in the presence of copper(II) chloride acts as a model reaction (Scheme 1).[10g,17a] An in-depth kinetic analysis based on steady-state and time-resolved emission, together with laser flash photolysis experiments, have provided key data to support the postulated mechanisms.

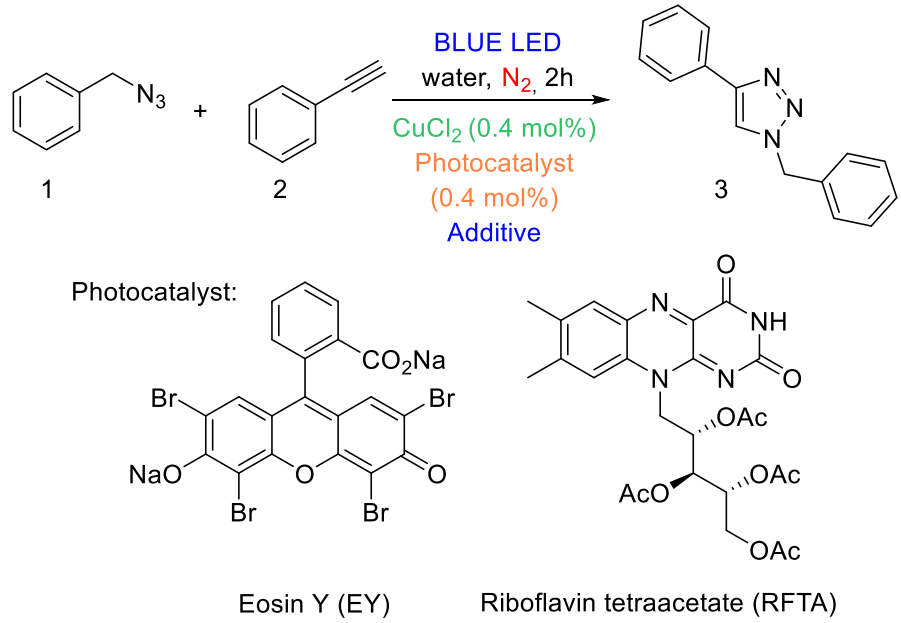

Scheme 1. Light-triggered CuAAC reaction system.

3. Results

3.1. Photochemical CuAAC reaction

The photocatalyzed reaction between benzyl azide (**1**) and phenyl acetylene (**2**) in the presence of copper (II) chloride under blue LED irradiation (3 W) for 2 h to produce 1,4-diphenyl-1,2,3-triazole **3** is shown in Scheme 1. The effect of different additives was evaluated, and the most relevant results collected in Table 1.

Table 1: Effect of the additives on the yield of CuAAC light-triggered by EY or RFTA.[a]

Entry	Photocatalyst (0.4 mol%)	Additive (mol%)	Yield of **3** (%)
1	**EY**	**-**	**93%**
2	EY	DABCO (1.2)	9%
3	EY	Et_3N (1.2)	23%
4	EY	NaN_3 (1.2)	86%
5	EY	NaN_3 (20)	35%
6[b]	EY	-	NR[c]
7	RFTA	-	20%
8	**RFTA**	**DABCO (1.2)**	**92%**
9	RFTA	DABCO (1.2)	35% (air)
10	RFTA	DABCO (1.2)	20% (O_2)
11	RFTA	Et_3N (1.2)	55%
12	RFTA	NaN_3 (1.2)	84%
13	RFTA	NaN_3 (20)	75%
14[b]	RFTA	-	NR[c]

[a]Reaction conditions: benzyl azide (**1**, 0.25 mmol) and phenyl acetylene (**2**, 0.25 mmol) in 2 mL of water under nitrogen atmosphere, irradiation with a 3 W blue LED for 2 h. $CuCl_2$ was used as a source of copper (0.4 mol%). Yields were obtained by GC using the internal standard method. [b]Dark reaction. [c]NR: no reaction.

When Cu(II) and EY at 0.4 mol% were used and the mixture was irradiated with a 3 W blue LED (λ_{exc} centered at 467 nm) for 2 h under inert atmosphere, **3** was obtained in a 93% yield (Table 1, entry 1). Afterwards, the effect of different sacrificial donors and sodium azide was investigated. The addition of DABCO or Et_3N (1.2 mol%) produced a dramatic decrease in the product formation, with the yield of **3** decreasing to 9% and 23%, respectively (Table 1, entries 2 and 3). Moreover, the addition of NaN_3 as an additive showed a small but definite quenching effect on the product formation, which was dependent on its concentration. In fact, the lower overall effect on the yield of **3** in

the presence of NaN_3, compared to the effect caused by Et_3N, could be due to a potential positive effect preventing the back electron transfer between $EY^{\bullet+}$ and Cu(I), associated to the anionic nature of the azide anion. Actually, the yield of product **3** decreased from 93% (no additive) to 86% (NaN_3 1.2 mol%), and even to 35 % (NaN_3 20 mol%) (Table 1, entries 1, 4 and 5). The photo-triggered CuAAC reaction using riboflavin tetraacetate (RFTA) as a redox-active chromophore was first reported by König et al.[17a] In our experiments, Cu(II) and RFTA were used at 0.4 mol%, affording a 20% yield of **3** under blue-LED light irradiation for 2 h under inert atmosphere (Table 1, entry 7). The significant difference in the performance of the two photocatalysts in the absence of additives (entries 1 and 7) deserves an explanation. In principle, the performance of two photocatalysts is not directly comparable since it depends on their respective absorbance at the given irradiation wavelength.[10b] Therefore, the efficiency of/in light absorption of EY and RFTA could explain their different photocatalytic activity. Nevertheless, absorption spectra of EY and RFTA recorded at the concentrations used for the CuAAC reaction (see figure S1) showed that absorbance at 467 nm is in both cases higher than 4. Thus, all the photons emitted by the blue LED employed were efficiently absorbed, pointing to a different behavior of the excited states of EY and RFTA to explain the different reactivity (*vide infra*).

As in the case of EY, the effect of different additives was investigated when CuAAC was light-triggered by RFTA. Only for the latter, the addition of DABCO, Et_3N, and sodium azide favored the product formation. Interestingly, the addition of 1.2 mol% of DABCO improved the reaction yield up to 92% (Table 1, entry 8); Et_3N also acted as a positive additive, even though its efficiency was significantly lower compared to DABCO, yielding 55% of **3** under the same reaction conditions (Table 1, entry 11). The performance of RFTA was sensitive to oxygen concentrations. In fact, when DABCO

was used as the additive in the presence of air or oxygen atmosphere, the triazole **3** production yield dropped to 35% and 20% yield, respectively, pointing to the participation of the triplet excited state of RFTA, more sensitive to O_2 than the singlet excited state (Table 1, entries 9 and 10). To our surprise, the azide anion, which is considered a typical quencher in photochemical reactions such as type II photooxidation, resulted to be a positive additive. Under the essayed concentrations, 1.2 and 20 mol%, triazole **3** was produced in 84% and 75 % yields, respectively (Table 1, entries 12 and 13). These results indicate that, although the presence of the NaN_3 as an additive is positive, its benefit is dropped at higher concentration of the sacrificial agent. Finally, there is no reaction under dark conditions for either photoredox catalysts (Table 1, entries 6 and 14). From optimized conditions (Table 1, entries 1 and 8), similar TON and TOF values were obtained for both photocatalyst: 23250 and 11625 h^{-1}, for EY; and 23000 and 11500 h^{-1} for RFTA. These results indicate that the CuAAC reaction efficiency is independent from the employed photocatalyst.

Preparative photolysis results indicated that the effect of additives commonly used in photoredox catalysis show opposite outcomes depending on the nature of the photocatalyst; while DABCO, Et_3N, and NaN_3 act as quenchers for EY, these additives boosted the reaction when it was light-triggered by RFTA. These contrasting observations indicate that the fundamental aspects and molecular basis of the mechanisms involved still remain poorly understood and deserve a deeper insight.

3.2. Photophysical measurements of EY

For experimental reasons, the kinetic measurements tried to mimic as much as possible the ‘standard’ reaction conditions (see Table 1). Despite the great value of carrying out organic synthesis reactions in water, CH_3CN/H_2O solvent mixture was used in kinetic determinations for technical and solubility reasons. Previous electrochemical study on

the Couple Cu(II)/Cu(I) did not show any change in both, redox potential and reversibility by the presence of a phenylacetylene-benzyl azide mixture[18], for this reason and the lack of reactivity in the dark, we have not considered these reagents in the photochemical study. Then, first we evaluated the potential reduction of Cu(II) to Cu(I) from the singlet and from the triplet excited states of EY. Steady-state fluorescence experiments revealed a slight interaction between the singlet excited state and Cu(II). Nevertheless, time-resolved emission experiments showed that ^{1}EY* is not quenched by Cu(II) (see Figure S2). Next, the potential of the triplet excited state to act as a reducing species was evaluated by means of laser flash photolysis (LFP) experiments. Initially, the transient absorption spectra of a deaerated solution of EY ($1x10^{-5}$ M) in CH_3CN:H_2O (99:1) was recorded both in the absence and in the presence of Cu(II), as shown in Figure 1.

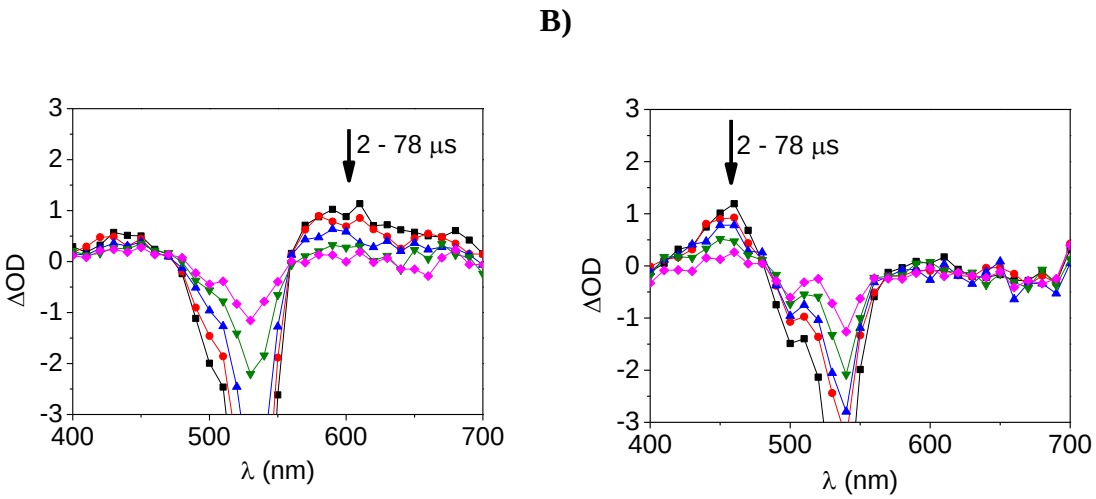

Figure 1: Transient absorption spectra of a solution of EY ($1x10^{-5}$ M in CH_3CN:H_2O (99:1)) recorded at different times: 2 μs (black), 10 μs (red), 22 μs (blue), 42 μs (green) and 78 μs (pink), after the laser pulse (λ_{exc} = 532 nm) in the absence (A), and in the presence (B) of Cu(II) ($1x10^{-3}$ M).

Figure 1A displays the characteristic transient absorption spectrum of the triplet excited state of the EY ($^3EY^*$) with a broad band range between 550-700 nm; by contrast, Figure 1B showed the spectrum characteristic of the radical cation ($EY^{\bullet+}$), with a distinctive maximum at 460 nm, obtained in the presence of Cu(II).[19] The formation of $EY^{\bullet+}$ upon addition of Cu(II) acted as an ambiguous evidence of the photoredox process. Moreover, the next step was the evaluation of the kinetic rate constant for the quenching of $^3EY^*$ by Cu(II). For this purpose, the decay traces corresponding to the triplet excited state, obtained upon LFP excitation, were evaluated at 580 nm at different concentrations of Cu(II) (Figure 2A). In parallel, traces were also recorded at 460 nm to account for the simultaneous formation of $EY^{\bullet+}$ (Figure 2B). Figure 2A shows an efficient decrease in the lifetime of $^3EY^*$ upon addition of increasing concentrations of Cu(II). Then, the reciprocal of the triplet lifetime was plotted *versus* [Cu(II)] according to the Stern-Volmer analysis (see experimental section 3.3). A quenching constant value of 2.9×10^9 $M^{-1}s^{-1}$, close to the diffusion control limit,[20] was determined from the slope of the Stern-Volmer plot (Table 2). Figure 2B shows the concomitant growth of the corresponding $EY^{\bullet+}$, in agreement with the observed triplet quenching.

A) **B)**

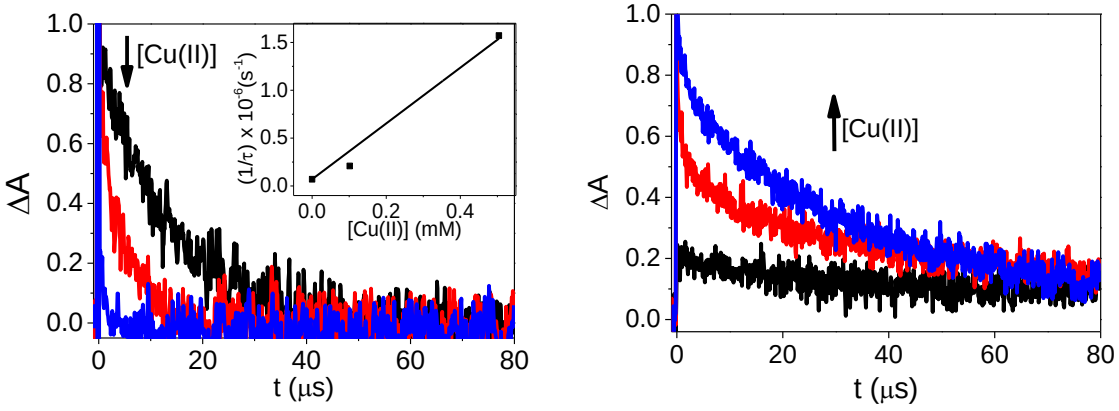

Figure 2: Kinetic traces recorded at 580 nm (A) and 460 nm (B), obtained upon LFP excitation (532 nm) of EY ($1x10^{-5}$ M in $CH_3CN:H_2O$ (99:1)) in the absence of Cu (black), and upon addition of Cu(II): $1x10^{-4}$ M (red) and $5x10^{-4}$ M (blue). Inset: corresponding Stern-Volmer plot.

The efficient quenching of the triplet excited state of EY, together with the concomitant formation of $EY^{\bullet+}$ upon addition of Cu(II), supported the triplet excited state of EY as the reducing agent of Cu(II).

Furthermore, Cl^- derived from HCl has been reported as a reducing agent for a different photocatalyst: 9-mesityl,10-methylacridinium.[21] Since we used $CuCl_2$ as a source of Cu(II), control experiments were performed to discard any photoredox reaction between the ground state or the excited states of EY and Cl^- (see Figure S3). For this purpose, NaCl was employed as Cl^- source. Nevertheless, UV-visible spectra, steady-state and time-resolved fluorescence revealed no interaction between Cl^- and EY nor with the ground state or with the singlet excited state of the dye. Furthermore, interaction between Cl^- and the triplet excited state of EY was also evaluated by LFP. Transient absorption spectrum revealed only a physical deactivation of $^3EY^*$ without electron transfer, since the corresponding $EY^{\bullet-}$ band, located at 400-430 nm, was not evidenced (see Figure S3).[19a] Therefore, electron transfer between Cl^- and $^3EY^*$ can be safely discarded.

Next, we evaluated the reactivity of the additives DABCO, Et_3N, and NaN_3 towards the excited states of EY. Initially, the interaction between the singlet excited state of EY and the electron donors (DABCO, Et_3N and NaN_3) was evaluated upon steady-state and time-resolved fluorescence experiments. Results showed a decrease in the steady-state emission and in the lifetime of $^1EY^*$ when DABCO was used as the electron donor, as shown in Figure 3. Then, the reciprocal of the fluorescence lifetime was plotted *versus*

[DABCO] (see experimental section). The slope of the Stern-Volmer fitting gave as result the kinetic constant value of $3.8x10^9$ $M^{-1}s^{-1}$, Table 2. Yet, results were different when Et_3N and NaN_3 were employed (see Figure S4). $^1EY^*$ remained unchanged in the presence of concentrations as high as $2x10^{-2}$ M of either of the two additives.

A) **B)**

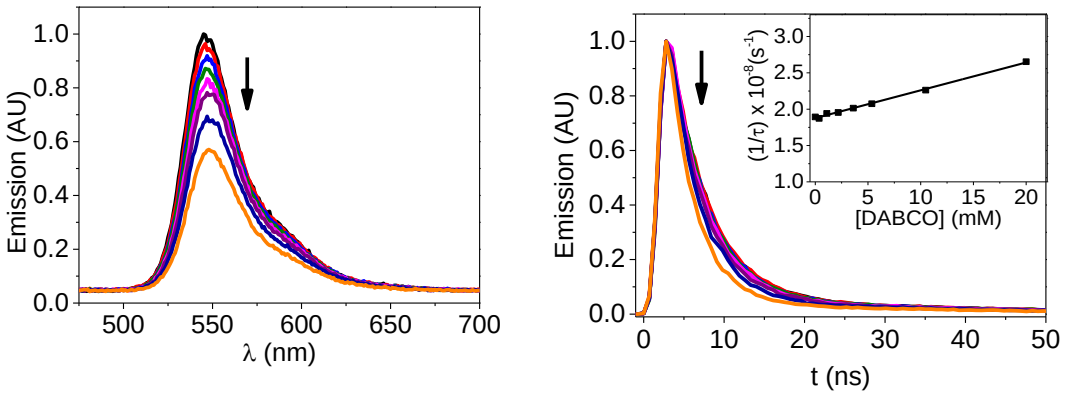

Figure 3: Steady-state (A) and time-resolved (B) fluorescence (λ_{exc} = 460 nm) of EY ($1x10^{-5}$ M) in CH_3CN:H_2O (99:1) upon addition of DABCO 0-$2x10^{-2}$ M. Inset: corresponding Stern-Volmer plot.

Conversely, when LFP experiments were carried out to evaluate the reactivity of the additives towards the $^3EY^*$, the results obtained showed that $^3EY^*$ lifetime decreased in the presence of increasing concentrations of the three electron donors (Figure 4). The corresponding quenching rate constant values, determined from the slopes of the linear fittings of the Stern-Volmer relationships, were $1.0x10^7$ $M^{-1}s^{-1}$, $7.6x10^6$ $M^{-1}s^{-1}$ and $3.1x10^7$ $M^{-1}s^{-1}$ for DABCO, Et_3N, and NaN_3, respectively (see Figures 4A, 4C and 4E and Table 2). As further support of the redox processes, the transient absorption spectrum of a deaerated solution of EY was recorded in the presence of DABCO ($2x10^{-2}$ M), as shown in Figure 4B. The formation of the radical anion of EY ($EY^{\bullet-}$), which is expected to give a band range between 400-430 nm, was observed as a clear indication

of the ability of excited EY to act also as an oxidant as well.[19a] Furthermore, traces recorded at 410 nm from deaerated solutions of EY in the absence and presence of Et_3N or NaN_3, also revealed the formation of $EY^{\bullet-}$ in these cases, as shown in Figures 4D and 4F, respectively.

A)

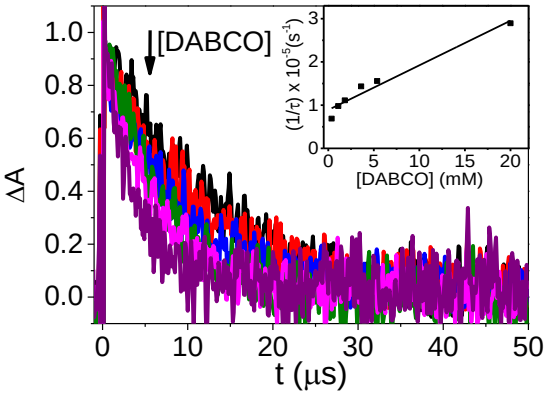

B)

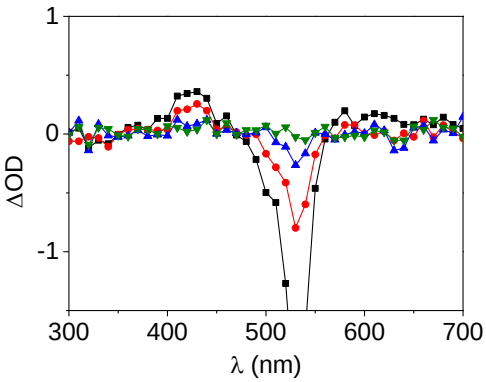

C)

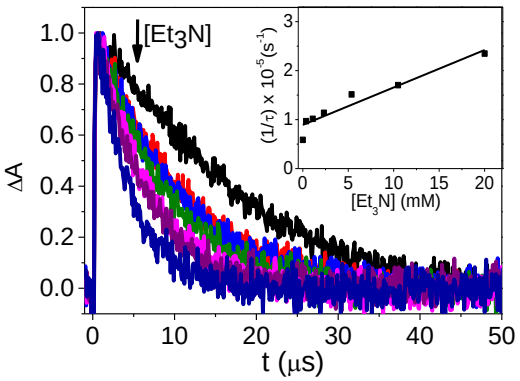

D)

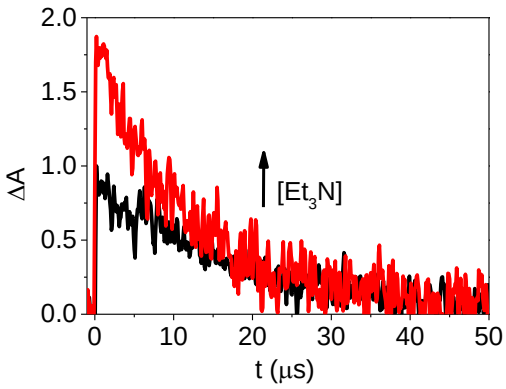

E)

F)

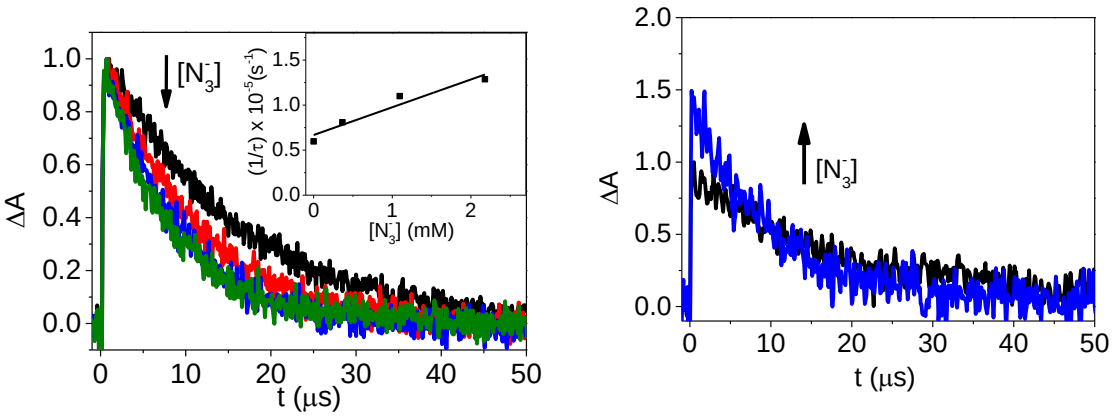

Figure 4: Kinetic traces obtained upon LFP excitation (λ_{exc} = 532 nm) of deaerated solutions of EY ($1x10^{-5}$ M) in $CH_3CN:H_2O$ (99:1), recorded at 580 nm upon addition of DABCO (up to $2x10^{-2}$ M, A), Et_3N (up to $2x10^{-2}$ M, C) and NaN_3 (up to $2.2x10^{-3}$ M, E). Insets: Stern-Volmer fittings corresponding to the quenching experiments. B) Transient absorption spectra obtained from a deaerated solution of EY in the presence of DABCO ($2x10^{-2}$ M) recorded at different times after the laser pulse: 6 μs (black), 14 μs (red), 30 μs (blue) and 78 μs (green). D and F) Kinetic traces recorded at 410 nm upon addition of Et_3N (up to $1.1x10^{-3}$ M) or NaN_3 (up to $1.1x10^{-3}$ M), respectively.

Table 2: Quenching rate constants determined for the reaction between the excited states of EY and the additives, together with the observed intermediates from the LFP measurements.

Quencher	k_{qS} **(M^{-1} s^{-1})**	k_{qT} **(M^{-1} s^{-1})**	***Observed Intermediate***
Cu(II)	-	$2.9x10^9$	$EY^{\bullet+}$
Cl^-	-	-	-
DABCO	$3.8x10^9$	$1.0x10^7$	$EY^{\bullet-}$

Et_3N	-	$7.6x10^6$	$EY^{\bullet-}$
NaN_3	-	$3.1x10^7$	$EY^{\bullet-}$

Finally, in order to assess the catalytic role of the copper salts used, we examined the reaction between the reduced Cu(I) and $EY^{\bullet+}$ to recover Cu(II) and EY. Thus, the kinetics of $EY^{\bullet+}$ (obtained from a solution containing EY and a large excess of $Cu(OAc)_2$) was examined upon addition of Cu(I); unfortunately, the experiment was not conclusive due to the low solubility of the Cu(I) salts.

3.3. Photophysical measurements with RFTA

The CuAAC photoinitiated by RFTA without additives only produced a 20% yield (Table 1), in contrast to the results obtained when EY was employed.[17c] In agreement with the experimental results, kinetic evaluation based on steady-state, time resolved fluorescence measurements and LFP experiments showed no interaction between the excited states of RFTA and Cu(II) (see Figure S5). Consequently, the reduction of Cu(II) to Cu(I) called for a more powerful reducing agent.

Quenching of the singlet excited state of riboflavin and amines, such as DABCO or Et_3N had been previously studied by our laboratory.[22] The quenching rate constants obtained were $4.5x10^9$ $M^{-1}s^{-1}$ and $2.9x10^9$ $M^{-1}s^{-1}$ for DABCO and Et_3N, respectively. Similarly, Figure 5 shows an efficient static and dynamic quenching of ^{1}RFTA* by NaN_3. Kinetic analysis based on the Stern-Volmer relationship resulted in a rate constant of $5.9x10^9$ $M^{-1}s^{-1}$ (see inset in Figure 5B and Table 3).

A) **B)**

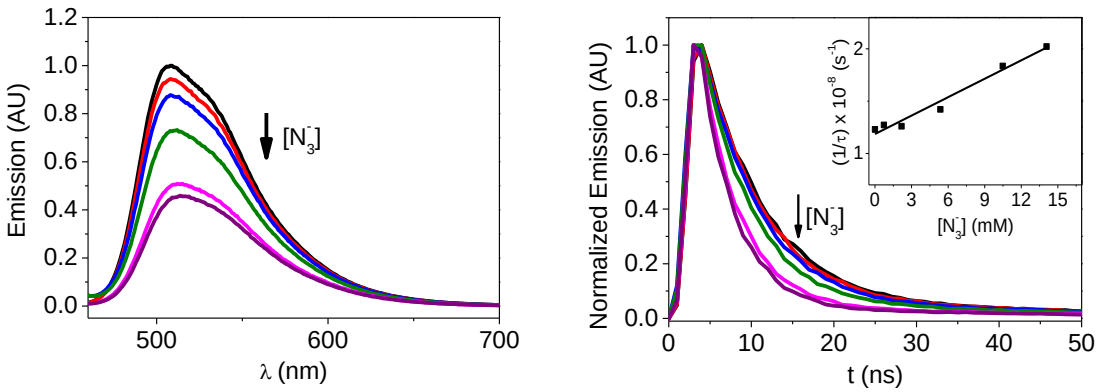

Figure 5: Quenching of steady-state (A) and time-resolved (B) fluorescence (λ_{exc} = 460 nm) of RFTA ($Abs_{\lambda=460\ nm}$ = 0.15 in CH_3CN), upon addition of NaN_3 (up to $1.4x10^{-2}$ M). Inset: Stern-Volmer fitting of the quenching experiment.

Next, the transient absorption spectra of a deaerated solution of RFTA showed a maximum centered at 380 nm and a wide band range between 500 and 700 nm, corresponding to the $^3RFTA^*$, in good agreement with the literature, see Figure 6.[22]

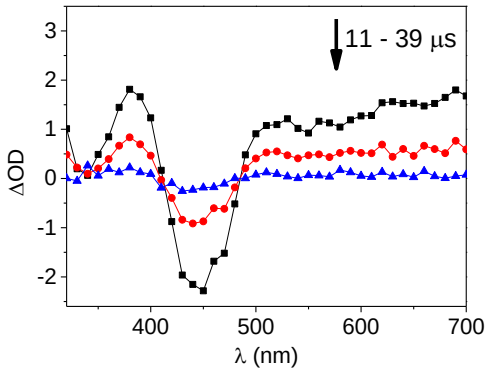

Figure 6: Transient absorption spectra of a deaerated CH_3CN solution of RFTA ($4x10^{-5}$ M) recorded at different times: 11 μs (black), 19 μs (red) and 39 μs (blue) after the laser pulse (λ_{exc} = 355 nm).

Subsequently, the lifetime of $^3RFTA^*$ was monitored at 620 nm upon increasing concentrations of DABCO, Et_3N, and NaN_3 (see Figures 7A, 7B and 7C, respectively).

The results revealed an efficient quenching of $^{3}RFTA^{*}$ in all cases. The lifetime decrease was plotted *versus* additive concentration according to the Stern-Volmer relationship (see insets in Figure 7). The slopes of the corresponding linear fittings provided the quenching constant values which were: $1.2x10^{10}$, $8.7x10^{8}$ and $7.3x10^{9}$ $M^{-1}s^{-1}$, for DABCO, Et_3N, and NaN_3, respectively (Table 3). The resulting spectra were recorded as further support of the electron transfer processes (Figure S6). As expected, in the case of Et_3N the resulting spectrum (Figure S6A) exhibited a strong absorption band located at 380 nm and a weak band between 500 and 650 nm, in agreement with the well-known $RFTAH^{\bullet}$, formed upon electron transfer followed by proton transfer from Et_3N to excited RFTA.[23] On the other hand, in the case of NaN_3 the spectrum corresponding to $RFTA^{\bullet-}$ was obtained as shown in Figure S6B. As expected, the latter is coincident with the already described spectrum of $RFTA^{\bullet-}$ obtained with DABCO.[22] Finally, traces recorded at 380 nm in the absence of and upon increasing concentrations of Et_3N (Figure 8A) or NaN_3 (Figure 8B) revealed the formation of the reduced species of RFTA ($RFTAH^{\bullet}$ or $RFTA^{\bullet-}$, respectively).

A)

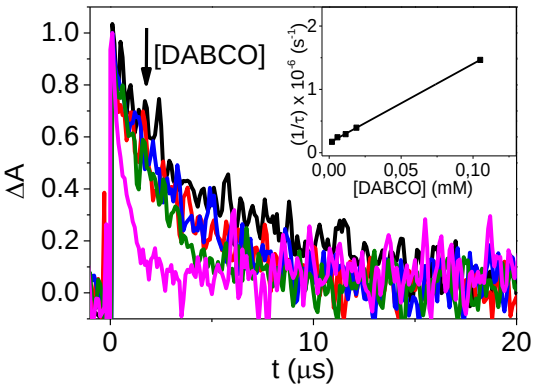

B)

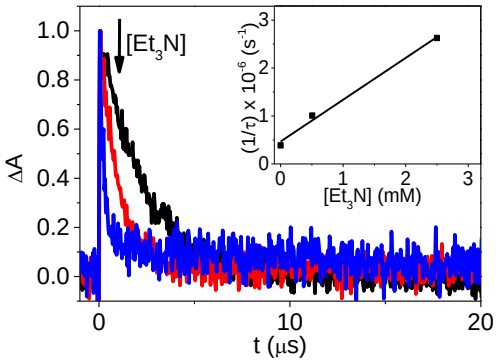

C)

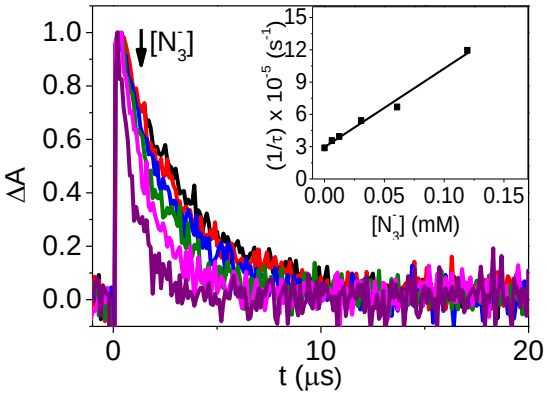

Figure 7: Kinetic traces obtained after LFP excitation (λ_{exc} = 355 nm) of RFTA ($4x10^{-5}$ M in deaerated CH_3CN), recorded at 620 nm upon addition of DABCO (up to $1.1x10^{-4}$ M, A), Et_3N (up to $2.5x10^{-3}$ M, B) or NaN_3 (up to $1.2x10^{-4}$ M, C). Inset: Stern-Volmer fittings of the corresponding quenching experiments.

A) **B)**

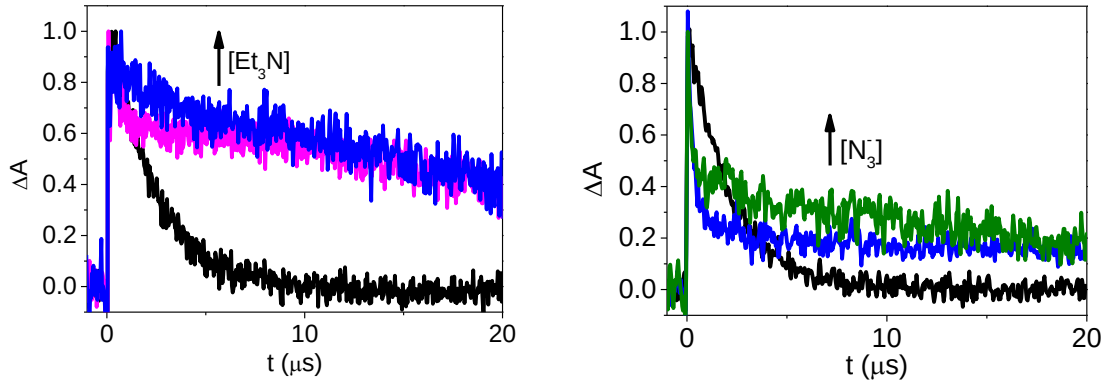

Figure 8: Kinetic traces obtained after LFP excitation (λ_{exc} = 355 nm) of RFTA ($4x10^{-5}$ M in deaerated CH_3CN), recorded at 380 nm upon addition of Et_3N (up to $2.5x10^{-3}$ M, A) or NaN_3 (up to $3x10^{-5}$, B).

Finally, we investigated the reduction of Cu(II) to Cu(I) by $RFTA^{\bullet-}$ or $RFTAH^{\bullet}$. Hence, a solution containing RFTA and DABCO or Et_3N was subjected to LFP excitation and the kinetic decay traces at 380 nm where $RFTA^{\bullet-}$ and $RFTAH^{\bullet}$ have strong absorptions

were recorded upon increasing concentrations of Cu(II) (see Figures 9A and 9B for the quenching of $RFTA^{\bullet-}$ and $RFTAH^{\bullet}$, respectively). The corresponding linear fittings based on the Stern-Volmer relationships were plotted in 9C and 9D, respectively.

Figures 9A and 9C revealed an efficient quenching of $RFTA^{\bullet-}$ by Cu(II), with a kinetic rate constant of 7.9×10^8 $M^{-1}s^{-1}$. Analogously, as shown in Figures 9B and 9D, $RFTAH^{\bullet}$ was also quenched by Cu(II), the slope of the linear fitting gave a quenching rate constant of 1.4×10^8 $M^{-1}s^{-1}$. The quenching rate constant values obtained are in agreement with the experimental results (see Table 1) that showed higher reaction yields in the presence of DABCO or NaN_3 (entries 8 and 12) compared to the yield obtained in the case of employing Et_3N as additive (entry 11).

A)

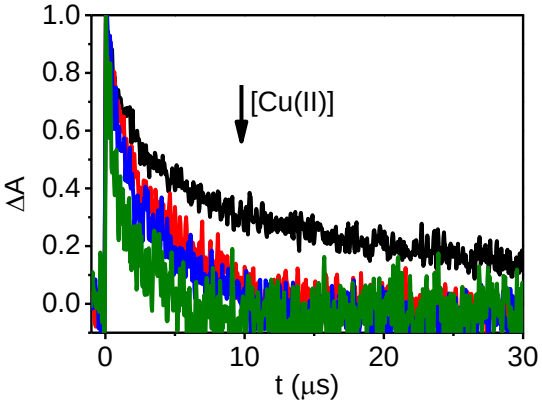

B)

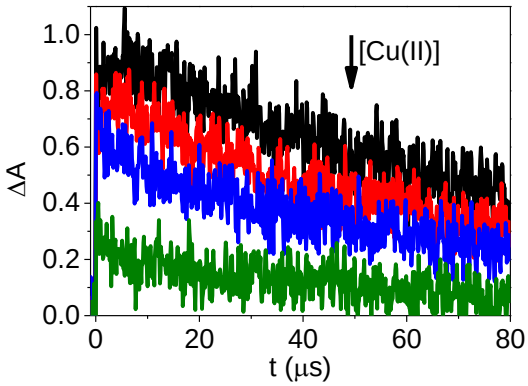

C)

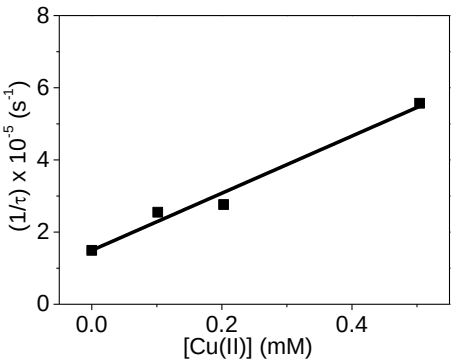

D)

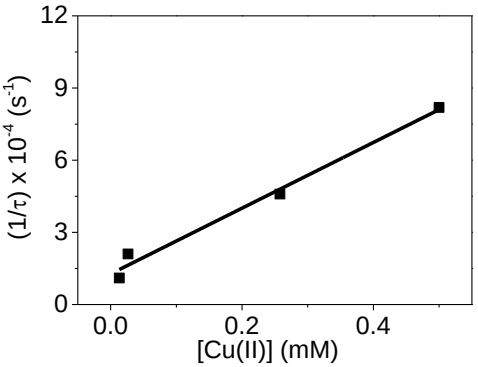

Figure 9: Decay traces obtained after LFP excitation (λ_{exc} = 355 nm) of a solution of RFTA ($4x10^{-5}$ M) and DABCO ($1x10^{-3}$ M, A) or Et_3N ($5x10^{-3}$ M, B) in deaerated CH_3CN, recorded at 380 nm upon addition of Cu(II) at a concentration up to $5x10^{-4}$ M. Corresponding Stern-Volmer plots for the reaction of Cu(II) towards (C) $RFTA^{\bullet-}$ or (D) $RFTAH^{\bullet}$.

Table 3: Quenching rate constants determined for the reaction between the excited states of RFTA or the derived reduced species and the additives, together with the observed intermediates from the LFP measurements.

Quencher	k_{qS} (M^{-1} s^{-1})	k_{qT} (M^{-1} s^{-1})	*Observed intermediate*	k_q *RFTA*$^{\bullet-}$ (M^{-1} s^{-1})	k_q *RFTAH*$^{\bullet}$ (M^{-1} s^{-1})
Cu(II)	-	-	-	$7.9x10^8$	$1.4x10^8$
DABCO	$4.5x10^{9, a}$	$1.2x10^{10}$	$RFTA^{\bullet-}$	-	-
Et_3N	$2.9x10^{9, a}$	$8.7x10^8$	$RFTAH^{\bullet}$	-	-
NaN_3	$5.9x10^9$	$7.3x10^9$	$RFTA^{\bullet-}$	-	-

[a]Data obtained from reference [22].

4. Discussion

Once the photocatalyst reached an excited state, the next step in a photoredox process is the electron transfer to form the corresponding radicals. The thermodynamic feasibility of that step was estimated by means of the Gibbs energy of photoinduced electron transfer equation:

$$\Delta G_{et}\ (eV) = -\ [\ E(A/A^{\bullet-}) - E(D^{\bullet+}/D)] - E_{S\ or\ T}{}^{*}\ (D\ or\ A) + \Delta E_{coulombic} \qquad \text{eq. 1}$$

where $E(A/A^{\bullet-})$ is the reduction potential of the acceptor species (A), $E(D^{\bullet+}/D)$ is the oxidation potential of the donor species (D), $E_{S\ or\ T}{}^{*}$ (D or A) is the energy of the singlet or triplet excited state of the photocatalyst, either acting as D or as A.[12b] In polar solvents, $\Delta E_{coulombic}$ is negligible (*ca*. 0.06 eV in CH_3CN)[10b] and is usually omitted in photophysical estimations, except when specific solvent effects are addressed.[11]

In our case, thermodynamic calculations were made to estimate the free energy changes of the expected steps involved in the CuAAC reaction photoinitiated by EY, using redox and photophysical reported data.

Reported redox potentials for EY are: $E(EY^{\bullet+}/EY)$ = +0.78 V *vs* SCE and $E(EY/EY^{\bullet-})$ = -1.06 V *vs* SCE, in CH_3CN:H_2O (1:1) and the excitation energy of $^1EY^*$ and $^3EY^*$ are 2.31 eV and 1.91 eV, respectively.[10b,24] It is widely accepted that upon excitation, EY can participate in oxidative and reductive quenching cycles. In our case, the exergonicity of the two alternatives was investigated by estimating the Gibbs free energies of the initial photoinduced electron transfer steps using the simplified version of the formerly known Rehm–Weller equation, that can be safely employed when reactions are performed in polar solvents.[11,25]

Furthermore, the Gibbs free energy was also estimated for the subsequent thermal steps.

For the oxidative quenching cycle, the corresponding processes involved are shown in equations 2 and 3, and for the reductive cycle the equations that apply are 4 and 5. In both cycles A accounts for Cu(II) and D accounts for DABCO, Et_3N, NaN_3, Cl^- or Cu(I).

Oxidative cycle:

$$\Delta G_{et}\ (eV) = -\ [\ E(A/A^{\bullet-}) - E(EY^{\bullet+}/EY)] - EY^{*} \qquad \text{eq. 2}$$

$$\Delta G\ (eV) = -\ [E(EY^{\bullet+}/EY) - E(D^{\bullet+}/D)] \qquad \text{eq. 3}$$

Reductive cycle:

$$\Delta G_{et}\ (eV) = -\ [\ E(EY/EY^{\bullet-}) - E(D^{\bullet+}/D)] - EY^{*} \qquad \text{eq. 4}$$

$$\Delta G\ (eV) = -\ [E(A/A^{\bullet-}) - E(EY/EY^{\bullet-})] \qquad \text{eq. 5}$$

Redox potential of Cu(II)/Cu(I) is 0.15 V *vs* SCE, thus reduction of Cu(II) from the $^{1}EY^{*}$ or $^{3}EY^{*}$ (eq. 2) gives free energy values of ΔG_{et} = -1.68 eV or ΔG_{et} = -1.28 eV, respectively. Subsequent oxidation of Cu(I) to Cu(II) by formed $EY^{\bullet+}$, according to equation 3, is also thermodynamically favored (ΔG = -0.63 eV), without the need of additives.

For the evaluation of the reductive cycle involvement, we estimated the free energy associated to the oxidation of DABCO, Et_3N, NaN_3 and Cl^- with redox potential values of +0.56 V, +0.96 V, +1.08 V and +1.15 V (all *vs* SCE),[20,26] respectively, from $^{1}EY^{*}$ and $^{3}EY^{*}$ (eq. 4). The estimated ΔG_{et} from the $^{1}EY^{*}$ are: ΔG_{et} = -0.69 eV, ΔG_{et} = -0.29 eV, ΔG_{et} = -0.17 eV and ΔG_{et} = -0.1 eV for DABCO, Et_3N, NaN_3 and Cl^-, respectively. The thermodynamic calculations for the oxidation of the electron donors involving the $^{3}EY^{*}$ indicated that the electron transfer is thermodynamically allowed only in the case of DABCO (ΔG_{et} = -0.29 eV), while such processes resulted endergonic for the rest of the additives (ΔG_{et} = +0.11 eV, ΔG_{et} = +0.23 eV and ΔG_{et} = +0.30 eV, for Et_3N, NaN_3 and Cl^-, respectively). Eventually, the reduction of Cu(II) from the $EY^{\bullet-}$ according to the thermal step depicted in equation 5, will be exergonic with ΔG = -1.21 eV.

An overall analysis of the thermodynamic estimations indicated that the $^{1}EY^{*}$ could not only be responsible for the reduction of Cu(II) but also for the oxidation of DABCO, Et_3N, NaN_3 and Cl^-. Yet, kinetic experiments based on time-resolved fluorescence showed that $^{1}EY^{*}$ lifetime remained constant upon addition of increasing concentrations of all of these reactants, except in the case of DABCO; therefore, the

participation of $^{1}EY^{*}$ in the photoreduction of Cu(II) was discarded. Nevertheless, LFP experiments showed that $^{3}EY^{*}$ lifetime was efficiently decreased upon addition of Cu(II) giving rise to the formation of $EY^{\bullet+}$, which acted as a piece of evidence of the participation of this excited state in the photoredox process. A control experiment showed that the $^{3}EY^{*}$ remained unchanged upon addition of Cl^{-} as a further support for the photoreduction of Cu(II), although $CuCl_2$ was used in the CuAAC. Yet, LFP experiments showed that the $^{3}EY^{*}$ was also quenched by DABCO, Et_3N or NaN_3, giving rise to the formation of $EY^{\bullet-}$, as demonstrated from the LFP experiments, even though thermodynamic estimations indicated that the oxidation of Et_3N and NaN_3 are slightly endergonic.

Albeit the quenching constant of the $^{3}EY^{*}$ by Cu(II) is at least two orders of magnitude higher than that measured for the additives (see Table 2), these results are in agreement with the decrease ~~of~~ in the yield of the CuAAC reaction in the presence of said additives. Special mention deserves the case of DABCO that also quenched the $^{1}EY^{*}$ with a high quenching rate constant, preventing partially the formation of the $^{3}EY^{*}$ and therefore decreasing significantly the yield of the CuAAC reaction. From the combination of the thermodynamic calculations and the kinetic experimental results, a plausible mechanism for this reaction is shown in Scheme 2, where a tiny amount of photo generated Cu(I) is able to catalyze the cycloaddition reaction (TON =2350) in competition to back electron transfer to regenerate EY.

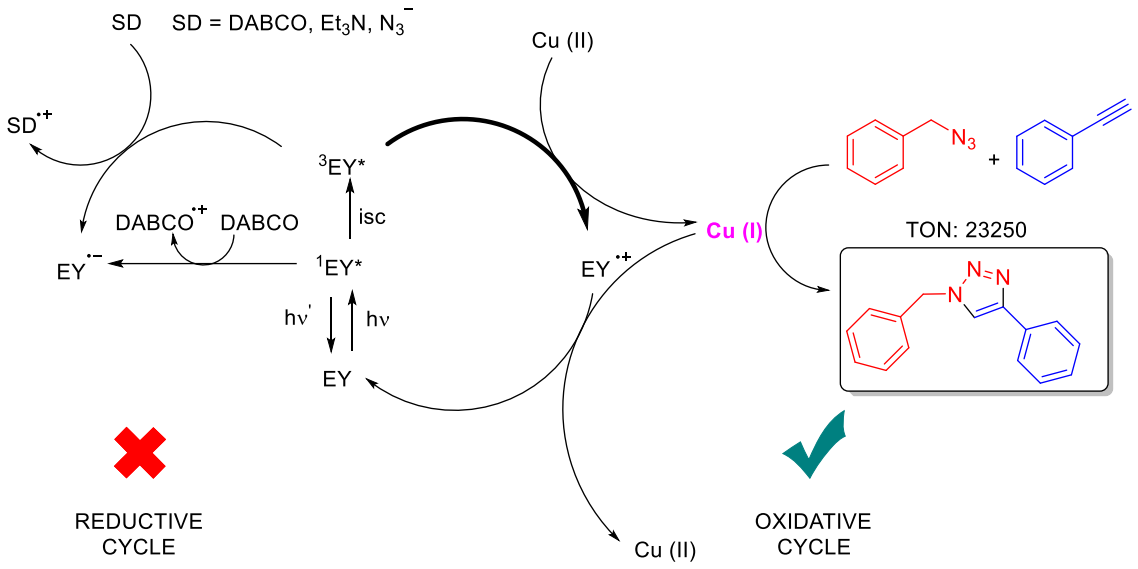

Scheme 2: Mechanistic proposal for the light-triggered CuAAC reaction by EY.

Analogously, thermodynamic estimations were made in the case of the CuAAC light-triggered by RFTA and were combined with the kinetic results to postulate a plausible reaction mechanism. Redox potentials for RFTA were safely taken as the redox potentials reported for RF, since the chromophore remained unchanged. These are: $E(RF^{\bullet+}/RF)$ = +2.03 V *vs* SCE[17c] and $E(RF/RF^{\bullet-})$ = -0.8 V *vs* SCE.[17b] In addition, the energies of the excited states of RFTA were assumed to be the same as the energies reported for the $^1RF^*$ and $^3RF^*$ (2.48 eV and 2.17 eV, respectively).[27]

From the thermodynamic point of view, reduction of Cu(II) was achieved from $^1RFTA^*$ and also from $^3RFTA^*$ (-0.6 eV and -0.29 eV, respectively, equation not shown). However, kinetic experiments showed that neither of the two excited states were able to reduce Cu(II). Nonetheless, oxidation of additives such as DABCO, Et_3N and NaN_3 were exergonic from the $^1RFTA^*$ (-1.12 eV, -0.72 eV and -0.6 eV, respectively), and also from the $^3RFTA^*$ (-0.81 eV, -0.41 eV and -0.29 eV, respectively), according to equation 6, where D accounts for DABCO, Et_3N or NaN_3. For these processes, kinetic experiments gave quenching rate constants close to the diffusion control from the $^1RFTA^*$ and from the $^3RFTA^*$, in agreement with the thermodynamic calculations.

Reductive cycle:

$$\Delta G_{et}\ (eV) = -\ [\ E(RFTA/RFTA^{\bullet-}) - E(D^{\bullet+}/D)] - RFTA^{*} \qquad \text{eq. 6}$$

$$\Delta G\ (eV) = -\ [E(A/A^{\bullet-}) - E(RFTA/RFTA^{\bullet-})] \qquad \text{eq. 7}$$

Once the RFTA was reduced, subsequent reduction of Cu(II) into Cu(I) according to the thermal redox process depicted in equation 7 (where A accounts for Cu(II)) is exergonic (-0.95 eV), which correlates well with the determined rate constant value in the order of 10^8 $M^{-1}s^{-1}$. The catalytic cycle could be closed by reoxidation of Cu(I) after participating in the CuAAC, by oxidized additives, which is also exergonic (-0.41 eV for DABCO as an example).

Albeit ^{1}RFTA* and ^{3}RFTA* demonstrated to play a role in the CuAAC reaction, the relative contribution of the two excited states can be stated applying equations S1-S5 (see SI) under real experimental conditions. Thus, concentrations of the additives ($1.5x10^{-3}$ M), the experimentally determined lifetimes values for ^{1}RFTA* and ^{3}RFTA* (τ_S = 8.3 ns and τ_T = 3.3 μs) the determined values for the quenching rate constants shown in Table 2, and the reported quantum yield values for RF Φ_F = 0.26 and Φ_{isc} = 0.70[28] were applied. Accordingly, quenching of the ^{1}RFTA* by DABCO, Et_3N and NaN_3 represented percentages of only 5.5%, 3.6% and 7.1%, respectively, while up to 68%, 57% and 66% of the ^{3}RFTA* was quenched by the electron donors at the concentrations employed. Furthermore, the yield of CuAAC light-triggered by RFTA was significantly affected by molecular oxygen (Table 1, entries 8-10), which is also in agreement with a higher participation of the ^{3}RFTA* over ^{1}RFTA*.

Overall, a plausible mechanism to explain the CuAAC reaction light-triggered by RFTA in the presence of electron donors is illustrated in Scheme 3.

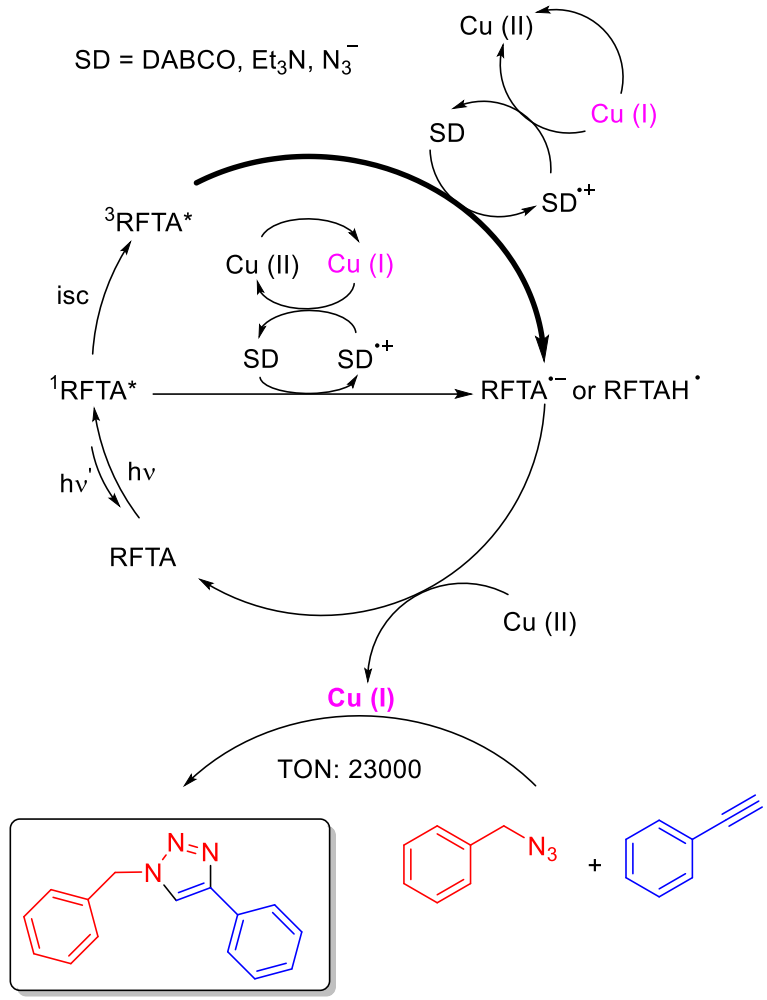

Scheme 3: Mechanistic proposal for the light-triggered CuAAC reaction by RFTA in the presence of DABCO, Et_3N and N_3^- as additives.

5. Conclusions

Experimental results obtained for the CuAAC model reaction photo-catalyzed by EY or RFTA in the presence of a series of additives were correlated with time-resolved photophysical experiments, which allowed determining the kinetic rate constants of the key steps. These results were combined with thermodynamic calculations to postulate plausible mechanisms for the CuAAC light-triggered by EY and RFTA. In the case of EY, Cu(II) was reduced by the $^3EY^*$, which was supported by the appearance of the transient spectrum of the resulting $EY^{\bullet+}$ recorded upon LFP excitation of EY in the presence of Cu(II); whereas in the case of RFTA, the initial photoreduction of the

photocatalyst by the electron donors used as additives afforded the reduced photocatalyst, $RFTA^{\bullet-}$ or $RFTAH^{\bullet}$. These reduced species were responsible for the reduction of Cu(II) in the next step. Time-resolved measurements supported the need or not of additives in the CuAAC reaction mediated by two different metal-free organic photocatalysts. The experimentally obtained kinetic data correlate well with thermodynamic estimations on the free energy changes associated to the key electron transfer steps.

We have demonstrated that time-resolved photophysical techniques provide key data to evaluate the behavior of the short-lived excited states of the photocatalysts. This approach constitutes a strong scientific pillar in the pathway to the optimization of photoredox processes rather than a random exploration of reaction conditions. We believe that it will help future researchers to save time in the design of new photoredox processes.

6. Experimental section

6.1 General procedures

Synthetic procedures and characterization data

General experimental procedure for the synthesis of 1-benzyl-4-phenyl-1*H*-1,2,3-triazole *via* visible-light promoted CuAAC reaction. The reactions were carried out in a 10 mL glass vial, equipped with a rubber septum and a magnetic stirrer. Benzyl azide (**1**, 0.25 mmol), phenyl acetylene (**2**, 0.25 mmol), and 1.6 mL of water were added. Next, 200 μL EY (5 mM) or RFTA (5 mM), 200 μL $CuCl_2$ (5 mM) and an additive such as DABCO (1.2 mol%), Et_3N (1.2 mol%), or NaN_3 (1.2 mol% and 20 mol%) were added and the mixture was purged with nitrogen for 15 min and then irradiated with a 3 W blue-LED (467 nm) for 2 h. Ethyl acetate (10 mL) and a saturated solution of $NaHCO_3$ (10 mL) were added and the mixture was stirred. The organic layer was separated, and the aqueous layer was extracted with ethyl acetate (2 × 10 mL). The combined organic extract was dried over anhydrous Na_2SO_4 and the yields of **3** were obtained by GC using internal standard method. Characterization was performed from

the pure triazole **3** isolated from the crude reaction mixture by flash column chromatography (silica gel, eluting with 1:1 pentane/dichloromethane (50 mL) and 1:1 dichloromethane/ethyl acetate (50 mL)).

1-benzyl-4-phenyl-1*H*-1,2,3-triazole (3): ^{1}H NMR (400 MHz, $CDCl_3$): δ = 5.58 (s, 2H), 7.31 – 7.33 (m, 3H), 7.37 – 7.42 (m, 5H), 7.66 (s, 1H), 7.80 (d, *J* = 7.2 Hz, 2H). $^{13}C\{^{1}H\}$ NMR (100 MHz, $CDCl_3$): δ = 54.4, 119.6, 125.9, 128.2, 128.3, 128.9, 129.3, 130.7, 134.9, 148.4.

Materials and Methods:

NaN_3, 1,4-diazabicyclo[2.2.2]octane (DABCO), *N*,*N*,*N*-triethylamine (Et_3N), eosin Y disodium salt (EY), CuCl, $CuCl_2$, $Cu(OAc)_2$, phenyl acetylene and benzyl azide are all high-purity commercial samples used without further purification. CH_3CN was HPLC grade from Scharlau and water was Milli-Q grade. Light-promoted reactions were performed in a borosilicate glass vial and employing a 3 W blue LED (LED High Power, Lambertian model, wavelength of peak intensity in 467 nm, luminous flux 22 lm, spectral distribution from 400 nm to 550 nm). The distance from the light source to the irradiation vessel was 1.0 cm and no filters were used. ^{1}H and $^{13}C\{^{1}H\}$ NMR spectra were recorded at 400.16 and 100.62 MHz respectively on a Bruker 400 spectrometer with $CDCl_3$ as a solvent. All spectra were reported in δ (ppm) relative to the residual solvent signal (δ_H ($CHCl_3$) = 7.26 ppm). Gas chromatographic analyses were performed on Agilent 5890 with a flame-ionization detector, on a 30 m capillary column of a 0.32 mm x 0.25 μm film thickness, with a 5% phenylpolysiloxane phase. GC-MS analyses were conducted on Agilent 7890 employing a 30 m x 0.25 mm x 0.25 μm with a 5% phenylpolysiloxane phase column. Riboflavin tetraacetate (RFTA) was prepared according to a well-established procedure.[29] The CuAAC reaction product, 1-benzyl-4-phenyl-1*H*-1,2,3-triazole, was isolated by flash column chromatography (silica gel, eluting with 1:1 pentane/dichloromethane (50 mL) and 1:1 dichloromethane/ethyl

acetate (50 mL)) from the reaction mixture and characterized by ^{1}H and ^{13}C NMR, and mass spectrometry. The isolated triazole spectroscopic data were in good agreement with those reported in literature.[10g]

6.2. Photophysical instrumentation

A Shimadzu UV-2101PC spectrophotometer was employed to obtain the UV/Vis absorption spectra.

Steady-state and time-resolved fluorescence experiments were performed on a Photon Technology International (PTI) LPS-220B spectrofluorometer and on an EasyLife V spectrofluorometer from OBB, respectively. In the case of time-resolved fluorescence, the excitation source was equipped with a pulsed LED (λ_{exc}=460 nm); the residual excitation signal was filtered in emission using a cut-off filter (50% transmission at 475 nm). Monoexponential decay functions that use a deconvolution procedure to separate from the lamp pulse profile provided the fitted kinetic traces.

A pulsed Nd: YAG SL404G-10 Spectron Laser Systems at the excitation wavelengths of 355 and 532 nm for RFTA and EY, respectively, was employed to carry out the laser flash photolysis (LFP) experiments. The energy of the single pulses (~10 ns duration) was lower than 15 mJ $pulse^{-1}$. The laser flash photolysis system was formed by the above-mentioned pulsed laser, a pulsed Lo255 Oriel Xenon lamp, a 77,200 Oriel monochromator, an Oriel photomultiplier tube (PMT) housing, a 70,705 PMT power supply and a TDS-640A Tektronix oscilloscope.

6.3. Photophysical experiments

Photophysical measurements were run at room temperature in quartz cells of 1 cm optical path length, using H_2O or CH_3CN:H_2O (99:1) as solvents for EY or CH_3CN for RFTA. For the steady-state and time-resolved fluorescence experiments, aerated

solutions of the photocatalyst (absorbance lower than 0.15 at λ_{exc}) were treated with increasing concentrations of the indicated quencher. Transient absorption measurements were recorded from deaerated solutions of the photocatalysts ($1x10^{-5}$ and $4x10^{-5}$ M for EY and RFTA, respectively) in the presence of the indicated quencher concentration.

The participation of the singlet excited states of the photocatalysts was evaluated from time-resolved fluorescence experiments carried out as a function of quencher concentrations. Analogously, the decay of the triplet excited state of EY and RFTA was monitored through laser flash photolysis measurements as a function of quencher concentration to determine the triplet quenching rate constants.

The same mathematical treatment was applied to the singlet and triplet excited states behavior as a function of quencher concentration. Thus, the lifetime of emission (for the singlet) or transient absorption (for the triplet) decays were fitted in all cases to the following monoexponential function:

$$y=A1\cdot*\exp(-x/\tau) + y0$$

where y represents the emission (or amplitude), x is the time, y0 is the offset and A1 represents the population of excited states of the photocatalyst with a specific lifetime (τ). (See Section S3 of the SI).

Next, quenching rate constants were determined according to the Stern-Volmer equation:

$$1/\tau = 1/\tau_o + k_q[Q]$$

where τ_o is the singlet (or triplet) lifetime of the photocatalyst in the absence of the quencher, τ is the lifetime of the photocatalyst in the presence of a given quencher concentration, and $[Q]$ is the quencher concentration. The quenching rate constants for the singlet (k_{qS}) and for the triplet excited states (k_{qT}) of EY or RFTA were the

corresponding slopes of the linear fittings of the Stern-Volmer plots. Besides, the R-square value of each Stern-Volmer plot is summarized in Table S1.

7. Associated content

Supporting Information, The Supporting Information is available free of charge at https://pubs.acs.org/

^{1}H-NMR, and ^{13}C{^{1}H}-NMR data, Photophysical experiments, Individual fittings, Equations (PDF)

8. Author information

Corresponding Authors:

Juan E. Argüello *- INFIQC-CONICET-UNC, Dpto. de Química Orgánica, Facultad de Ciencias Químicas, Universidad Nacional de Córdoba, Ciudad Universitaria, X5000HUA Córdoba, Argentina; orcid.org/0000-0002-7321-4291*

e-mail: jea@fcq.unc.edu.ar

M. Luisa Marin *- Instituto de Tecnología Química, Universitat Politècnica de València-Consejo Superior de Investigaciones Científicas, Avenida de los Naranjos s/n, 46022 Valencia, Spain; orcid.org/0000-0002-9789-8894*

e-mail: marmarin@qim.upv.es

Authors:

Rebeca Martínez-Haya *- Instituto de Tecnología Química, Universitat Politècnica de València-Consejo Superior de Investigaciones Científicas, Avenida de los Naranjos s/n, 46022 Valencia, Spain; orcid.org/ 0000-0002-2680-2998*

Adrián A. Heredia *- INFIQC-CONICET-UNC, Dpto. de Química Orgánica, Facultad de Ciencias Químicas, Universidad Nacional de Córdoba, Ciudad Universitaria, X5000HUA Córdoba, Argentina; orcid.org/0000-0002-2242-8855*

Willber D. Castro-Godoy *- Departamento de Química, Física y Matemática, Facultad de Química y Farmacia, Universidad de El Salvador, Final Av. de Mártires y Héroes del 30 de Julio, San Salvador 1101, El Salvador; orcid.org/0000-0001-7484-1644*

Luciana C. Schmidt *- INFIQC-CONICET-UNC, Dpto. de Química Orgánica, Facultad de Ciencias Químicas, Universidad Nacional de Córdoba, Ciudad Universitaria, X5000HUA Córdoba, Argentina; orcid.org/0000-0001-7059-3938*

Complete contact information is available at: https://pubs.acs.org/

Notes: The authors declare no competing financial interest.

9. Dedication

Dedicated in memory of Professor Jean-Michel Savéant (Université Paris 7 - Denis Diderot)

10. . Acknowledgments

We acknowledge financial support from the Spanish Government (Grant SEV-2016-0683), the Spanish Ministry of Science, Innovation and Universities (Project PID2019-110441RB-C33), the Generalitat Valenciana (Prometeo 2017/075), the Generalitat Valenciana, and the European Social Fund for postdoctoral contract (APOSTD2019-124 for R. M-H.). R. M-H. We would also like to thank the financial support for a predoctoral contract from Apadrina la Ciencia Association and Ford España/Ford Motor Company Fund. We also acknowledge INFIQC-CONICET and Universidad Nacional de Córdoba (UNC). This work was partly supported by CONICET, SECyT-UNC, and FONCyT.

11. References

(1) (a) Marzo, L.; Pagire, S. K.; Reiser, O.; König, B. Visible-Light Photocatalysis: Does It Make a Difference in Organic Synthesis? *Angew. Chem. Int. Ed.* **2018**, *57*, 10034-10072. (b) Arias-Rotondo, D. M.; McCusker, J. K. The photophysics of photoredox catalysis: a roadmap for catalyst design. *Chem. Soc. Rev.* **2016**, *45*, 5803-5820.
(2) (a) McAtee, R. C.; McClain, E. J.; Stephenson, C. R. J. Illuminating Photoredox Catalysis. *Trends Chem.* **2019**, *1*, 111-125. (b) Nguyen, J. D.; Tucker, J. W.; Konieczynska, M. D.; Stephenson, C. R. J. Intermolecular Atom Transfer Radical Addition to Olefins Mediated by Oxidative Quenching of Photoredox Catalysts. *J. Am. Chem. Soc.* **2011**, *133*, 4160-4163. (c) Wallentin, C.-J.; Nguyen, J. D.; Finkbeiner, P.; Stephenson, C. R. J. Visible Light-Mediated Atom Transfer Radical Addition via Oxidative and Reductive Quenching of Photocatalysts. *J. Am. Chem. Soc.* **2012**, *134*, 8875-8884. (d) Goliszewska, K.; Rybicka-Jasińska, K.; Clark, J. A.; Vullev, V. I.; Gryko, D. Photoredox Catalysis: The Reaction Mechanism Can Adjust to Electronic Properties of a Catalyst. *ACS Catal.* **2020**, *10*, 5920-5927.
(3) (a) Rani, A.; Singh, G.; Singh, A.; Maqbool, U.; Kaur, G.; Singh, J. CuAAC-ensembled 1,2,3-triazole-linked isosteres as pharmacophores in drug discovery: review. *RSC Adv.* **2020**, *10*,

5610-5635. (b) Bonandi, E.; Christodoulou, M. S.; Fumagalli, G.; Perdicchia, D.; Rastelli, G.; Passarella, D. The 1,2,3-triazole ring as a bioisostere in medicinal chemistry. *Drug Discov. Today* **2017**, *22*, 1572-1581. (c) Prachayasittikul, V.; Pingaew, R.; Anuwongcharoen, N.; Worachartcheewan, A.; Nantasenamat, C.; Prachayasittikul, S.; Ruchirawat, S.; Prachayasittikul, V. Discovery of novel 1,2,3-triazole derivatives as anticancer agents using QSAR and in silico structural modification. *SpringerPlus* **2015**, *4*, 571. (d) Lauria, A.; Delisi, R.; Mingoia, F.; Terenzi, A.; Martorana, A.; Barone, G.; Almerico, A. M. 1,2,3-Triazole in Heterocyclic Compounds, Endowed with Biological Activity, through 1,3-Dipolar Cycloadditions. *Eur. J. Org. Chem.* **2014**, *2014*, 3289-3306. (e) Huo, J.; Hu, Z.; Chen, D.; Luo, S.; Wang, Z.; Gao, Y.; Zhang, M.; Chen, H. Preparation and Characterization of Poly-1,2,3-triazole with Chiral 2(5H)-Furanone Moiety as Potential Optical Brightening Agents. *ACS Omega* **2017**, *2*, 5557-5564. (f) Wang, Z.; Tao, Y.; Wang, Z.; Yan, J. Synthesis and characterization of poly(N-vinyl-1,2,3-triazole)s derived from monomers obtained by highly efficient Wolff's cyclocondensation. *Polym. Chem.* **2016**, *7*, 3172-3178. (g) Kantheti, S.; Narayan, R.; Raju, K. V. S. N. The impact of 1,2,3-triazoles in the design of functional coatings. *RSC Adv.* **2015**, *5*, 3687-3708.

(4) (a) Meldal, M.; Tornøe, C. W. Cu-Catalyzed Azide−Alkyne Cycloaddition. *Chem. Rev.* **2008**, *108*, 2952-3015. (b) Hein, J. E.; Fokin, V. V. Copper-catalyzed azide–alkyne cycloaddition (CuAAC) and beyond: new reactivity of copper(i) acetylides. *Chem. Soc. Rev.* **2010**, *39*, 1302-1315. (c) Tiwari, V. K.; Mishra, B. B.; Mishra, K. B.; Mishra, N.; Singh, A. S.; Chen, X. Cu-Catalyzed Click Reaction in Carbohydrate Chemistry. *Chem. Rev.* **2016**, *116*, 3086-3240. (d) Singh, M. S.; Chowdhury, S.; Koley, S. Advances of azide-alkyne cycloaddition-click chemistry over the recent decade. *Tetrahedron* **2016**, *72*, 5257-5283. (e) Haldón, E.; Nicasio, M. C.; Pérez, P. J. Copper-catalysed azide–alkyne cycloadditions (CuAAC): an update. *Org. Biomol. Chem.* **2015**, *13*, 9528-9550. (f) Totobenazara, J.; Burke, A. J. New click-chemistry methods for 1,2,3-triazoles synthesis: recent advances and applications. *Tetrahedron Lett.* **2015**, *56*, 2853-2859. (g) Berg, R.; Straub, B. F. Advancements in the mechanistic understanding of the copper-catalyzed azide–alkyne cycloaddition. *Beilstein J. Org. Chem.* **2013**, *9*, 2715-2750. (h) Nebra, N.; García-Álvarez, J. Recent Progress of Cu-Catalyzed Azide-Alkyne Cycloaddition Reactions (CuAAC) in Sustainable Solvents: Glycerol, Deep Eutectic Solvents, and Aqueous Media. *Molecules* **2020**, *25*, 2015.

(5) (a) Rostovtsev, V. V.; Green, L. G.; Fokin, V. V.; Sharpless, K. B. A Stepwise Huisgen Cycloaddition Process: Copper(I)-Catalyzed Regioselective "Ligation" of Azides and Terminal Alkynes. *Angew. Chem. Int. Ed.* **2002**, *41*, 2596-2599. (b) Tornøe, C. W.; Christensen, C.; Meldal, M. Peptidotriazoles on Solid Phase: [1,2,3]-Triazoles by Regiospecific Copper(I)-Catalyzed 1,3-Dipolar Cycloadditions of Terminal Alkynes to Azides. *J. Org. Chem.* **2002**, *67*, 3057-3064.

(6) (a) Tasdelen, M. A.; Yagci, Y. Light-Induced Click Reactions. *Angew. Chem. Int. Ed.* **2013**, *52*, 5930-5938. (b) Bear, J. C.; Hollingsworth, N.; McNaughter, P. D.; Mayes, A. G.; Ward, M. B.; Nann, T.; Hogarth, G.; Parkin, I. P. Copper-Doped CdSe/ZnS Quantum Dots: Controllable Photoactivated Copper(I) Cation Storage and Release Vectors for Catalysis. *Angew. Chem. Int. Ed.* **2014**, *53*, 1598-1601. (c) Beniazza, R.; Lambert, R.; Harmand, L.; Molton, F.; Duboc, C.; Denisov, S.; Jonusauskas, G.; McClenaghan, N. D.; Lastécouères, D.; Vincent, J.-M. Sunlight-Driven Copper-Catalyst Activation Applied to Photolatent Click Chemistry. *Chem. Eur. J.* **2014**, *20*, 13181-13187. (d) Yetiskin, O.; Dadashi-Silab, S.; Khan, S. B.; Asiri, A. M.; Yagci, Y. Visible-Light-Induced Copper(I)-Catalyzed Azide-Alkyne Cycloaddition Initiated by Zinc Oxide Semiconductor Nanoparticles. *Asian J. Org. Chem.* **2015**, *4*, 442-444. (e) Wang, B.; Durantini, J.; Nie, J.; Lanterna, A. E.; Scaiano, J. C. Heterogeneous Photocatalytic Click Chemistry. *J. Am. Chem. Soc.* **2016**, *138*, 13127-13130. (f) Kumar, G. S.; Lin, Q. Light-Triggered Click Chemistry. *Chem. Rev.* **2020** IN PRESS.

(7) Adzima, B. J.; Tao, Y.; Kloxin, C. J.; DeForest, C. A.; Anseth, K. S.; Bowman, C. N. Spatial and temporal control of the alkyne–azide cycloaddition by photoinitiated Cu(II) reduction. *Nat. Chem.* **2011**, *3*, 256-259.

(8) (a) Harmand, L.; Lambert, R.; Scarpantonio, L.; McClenaghan, N. D.; Lastécouères, D.; Vincent, J.-M. A Photoreducible Copper(II)-Tren Complex of Practical Value: Generation of a Highly Reactive Click Catalyst. *Chem. Eur. J.* **2013**, *19*, 16231-16239. (b) Dadashi-Silab, S.; Yagci, Y. Copper (II) thioxanthone carboxylate as a photoswitchable photocatalyst for photoinduced click chemistry. *Tetrahedron Lett.* **2015**, *56*, 6440-6443. (c) Guan, X.; Zhang, J.; Wang, Y. An efficient photocatalyst for the azide–alkyne click reaction based on direct photolysis of a copper (II)/carboxylate complex. *Chem. Lett.* **2014**, *43*, 1073-1074. (d) Alzahrani, A. A.; Erbse, A. H.; Bowman, C. N. Evaluation and development of novel photoinitiator complexes for photoinitiating the copper-catalyzed azide–alkyne cycloaddition reaction. *Polym. Chem.* **2014**, *5*, 1874-1882. (e) Tasdelen, M. A.; Yagci, Y. Light-induced copper (I)-catalyzed click chemistry. *Tetrahedron Lett.* **2010**, *51*, 6945-6947. (f) Fayad, R.; Engl, S.; Danilov, E. O.; Hauke, C. E.; Reiser, O.; Castellano, F. N. Direct Evidence of Visible Light-Induced Homolysis in Chlorobis(2,9-dimethyl-1,10-phenanthroline)copper(II). *J. Phys. Chem. Lett.* **2020**, *11*, 5345-5349. (g) Abderrazak, Y.; Bhattacharyya, A.; Reiser, O. Visible-Light-Induced Homolysis of Earth-Abundant Metal-Substrate Complexes: A Complementary Activation Strategy in Photoredox Catalysis. *Angew. Chem. Int. Ed.* **2021** IN PRESS.

(9) (a) Kumar, P.; Joshi, C.; Srivastava, A. K.; Gupta, P.; Boukherroub, R.; Jain, S. L. Visible Light Assisted Photocatalytic [3 + 2] Azide–Alkyne "Click" Reaction for the Synthesis of 1,4-Substituted 1,2,3-Triazoles Using a Novel Bimetallic Ru–Mn Complex. *ACS Sustain. Chem. Eng.* **2016**, *4*, 69-75. (b) Hardy, M. D.; Konetski, D.; Bowman, C. N.; Devaraj, N. K. Ruthenium photoredox-triggered phospholipid membrane formation. *Org. Biomol. Chem.* **2016**, *14*, 5555-5558. (c) Yilmaz, G.; Iskin, B.; Yagci, Y. Photoinduced Copper(I)-Catalyzed Click Chemistry by the Electron Transfer Process Using Polynuclear Aromatic Compounds. *Macromol. Chem. Phys.* **2014**, *215*, 662-668.

(10) (a) Bouchet, L. M.; Heredia, A. A.; Argüello, J. E.; Schmidt, L. C. Riboflavin as Photoredox Catalyst in the Cyclization of Thiobenzanilides: Synthesis of 2-Substituted Benzothiazoles. *Org. Lett.* **2020**, *22*, 610-614. (b) Romero, N. A.; Nicewicz, D. A. Organic Photoredox Catalysis. *Chem. Rev.* **2016**, *116*, 10075-10166. (c) Meyer, A. U.; Straková, K.; Slanina, T.; König, B. Eosin Y (EY) Photoredox-Catalyzed Sulfonylation of Alkenes: Scope and Mechanism. *Chem. A Eur. J.* **2016**, *22*, 8694-8699. (d) Hari, D. P.; König, B. Synthetic applications of eosin Y in photoredox catalysis. *Chem. Commun.* **2014**, *50*, 6688-6699. (e) Ravelli, D.; Fagnoni, M. Dyes as Visible Light Photoredox Organocatalysts. *ChemCatChem* **2012**, *4*, 169-171. (f) Srivastava, V.; Singh, P. P. Eosin Y catalysed photoredox synthesis: a review. *RSC Advances* **2017**, *7*, 31377-31392. (g) Castro-Godoy, W. D.; Heredia, A. A.; Schmidt, L. C.; Argüello, J. E. A straightforward and sustainable synthesis of 1,4-disubstituted 1,2,3-triazoles via visible-light-promoted copper-catalyzed azide–alkyne cycloaddition (CuAAC). *RSC Adv.* **2017**, *7*, 33967-33973.

(11) Pitre, S. P.; McTiernan, C. D.; Scaiano, J. C. Understanding the Kinetics and Spectroscopy of Photoredox Catalysis and Transition-Metal-Free Alternatives. *Acc. Chem. Res.* **2016**, *49*, 1320-1330.

(12) (a) Buzzetti, L.; Crisenza, G. E. M.; Melchiorre, P. Mechanistic Studies in Photocatalysis. *Angew. Chem. Int. Ed.* **2019**, *58*, 3730-3747. (b) Marin, M.; Miranda, M. A.; Marin, M. L. A comprehensive mechanistic study on the visible-light photocatalytic reductive dehalogenation of haloaromatics mediated by Ru (bpy) 3 Cl 2. *Catal. Sci. Technol.* **2017**, *7*, 4852-4858.

(13) (a) Yagci, Y.; Tasdelen, M. A.; Jockusch, S. Reduction of Cu(II) by photochemically generated phosphonyl radicals to generate Cu(I) as catalyst for atom transfer radical polymerization and azide-alkyne cycloaddition click reactions. *Polymer* **2014**, *55*, 3468-3474. (b) Chibac, A. L.; Melinte, V.; Brezová, V.; Renard, E.; Brosseau, A.; Langlois, V.; Versace, D.-L. Metal-Free and Heterogeneous Photocatalytic Reduction of 4-Nitroaniline by a Poly(Ethylene Glycol)-Supported Eosin Dye under Visible-Light Exposure. *ChemCatChem* **2019**, *11*, 3307-3317.

(14) (a) El-Zaatari, B. M.; Shete, A. U.; Adzima, B. J.; Kloxin, C. J. Towards understanding the kinetic behaviour and limitations in photo-induced copper(i) catalyzed azide–alkyne

cycloaddition (CuAAC) reactions. *Phys. Chem. Chem. Phys.* **2016**, *18*, 25504-25511. (b) El-Zaatari, B. M.; Cole, S. M.; Bischoff, D. J.; Kloxin, C. J. Copper ligand and anion effects: controlling the kinetics of the photoinitiated copper(i) catalyzed azide—alkyne cycloaddition polymerization. *Polym. Chem.* **2018**, *9*, 4772-4780.
(15) Jennah, O.; Beniazza, R.; Lozach, C.; Jardel, D.; Molton, F.; Duboc, C.; Buffeteau, T.; El Kadib, A.; Lastécouères, D.; Lahcini, M.; Vincent, J.-M. Photoredox Catalysis at Copper(II) on Chitosan: Application to Photolatent CuAAC. *Adv. Synth. Catal.* **2018**, *360*, 4615-4624.
(16) (a) Decan, M. R.; Impellizzeri, S.; Marin, M. L.; Scaiano, J. C. Copper nanoparticle heterogeneous catalytic 'click' cycloaddition confirmed by single-molecule spectroscopy. *Nat. Commun.* **2014**, *5*, 4612. (b) Wang, B.; Lanterna, A. E.; Scaiano, J. C. Click Chemistry: Mechanistic Insights into the Role of Amines Using Single-Molecule Spectroscopy. *ACS Catal.* **2017**, *7*, 8487-8492.
(17) (a) Ritter, S. C.; König, B. Signal amplification and transduction by photo-activated catalysis. *Chem. Commun.* **2006**, 4694-4696. (b) Porcal, G.; Bertolotti, S. G.; Previtali, C. M.; Encinas, M. V. Electron transfer quenching of singlet and triplet excited states of flavins and lumichrome by aromatic and aliphatic electron donors. *Phys. Chem. Chem. Phys.* **2003**, *5*, 4123-4128. (c) Lu, C.; Lin, W.; Wang, W.; Han, Z.; Yao, S.; Lin, N. Riboflavin (VB2) photosensitized oxidation of *2′*-deoxyguanosine-*5′*-monophosphate (dGMP) in aqueous solution: a transient intermediates study. *Phys. Chem. Chem. Phys.* **2000**, *2*, 329-334.
(18) Hong, V.; Udit, A. K.; Evans, R. A.; Finn, M. G. Electrochemically Protected Copper(I)-Catalyzed Azide–Alkyne Cycloaddition. *ChemBioChem* **2008**, *9*, 1481-1486.
(19) (a) Yang, D.-T.; Meng, Q.-Y.; Zhong, J.-J.; Xiang, M.; Liu, Q.; Wu, L.-Z. Metal-Free Desulfonylation Reaction Through Visible-Light Photoredox Catalysis. *Eur. J. Org. Chem.* **2013**, 7528-7532. (b) Islam, S. D.-M.; Konishi, T.; Fujitsuka, M.; Ito, O.; Nakamura, Y.; Usui, Y. Photosensitized Reduction of Methyl Viologen Using Eosin-Y in Presence of a Sacrificial Electron Donor in Water–Alcohol Mixture. *Photochem. Photobiol.* **2000**, *71*, 675-680.
(20) Murov, S. L.; Carmichael, I.; Hug, G. L. *Handbook of Photochemistry, 2nd ed.*; Marcel Dekker: New York, 2009.
(21) Ohkubo, K.; Fujimoto, A.; Fukuzumi, S. Metal-free oxygenation of cyclohexane with oxygen catalyzed by 9-mesityl-10-methylacridinium and hydrogen chloride under visible light irradiation. *Chem. Commun.* **2011**, *47*, 8515-8517.
(22) Martinez-Haya, R.; Miranda, M. A.; Marin, M. L. Metal-Free Photocatalytic Reductive Dehalogenation Using Visible-Light: A Time-Resolved Mechanistic Study. *Eur. J. Org. Chem.* **2017**, *2017*, 2164-2169.
(23) (a) Bertolotti, S. G.; Previtali, C. M.; Rufs, A. M.; Encinas, M. V. Riboflavin/Triethanolamine as Photoinitiator System of Vinyl Polymerization. A Mechanistic Study by Laser Flash Photolysis. *Macromolecules* **1999**, *32*, 2920-2924. (b) Diaz, M.; Luiz, M.; Alegretti, P.; Furlong, J.; Amat-Guerri, F.; Massad, W.; Criado, S.; Garcia, N. A. Visible-light-mediated photodegradation of 17 beta-estradiol: Kinetics, mechanism and photoproducts. *J. Photochem. Photobiol., A* **2009**, *202*, 221-227. (c) Pajares, A.; Bregliani, M.; Montana, M. P.; Criado, S.; Massad, W.; Gianotti, J.; Gutierrez, I.; Garcia, N. A. Visible-light promoted photoprocesses on aqueous gallic acid in the presence of riboflavin. Kinetics and mechanism. *J. Photochem. Photobiol., A* **2010**, *209*, 89-94.
(24) Lazarides, T.; McCormick, T.; Du, P.; Luo, G.; Lindley, B.; Eisenberg, R. Making Hydrogen from Water Using a Homogeneous System Without Noble Metals. *J. Am. Chem. Soc.* **2009**, *131*, 9192-9194.
(25) (a) Rehm, D.; Weller, A. Kinetics of fluorescence quenching by electron and H-atom transfer. *Isr. J. Chem.* **1970**, *8*, 259-271. (b) Braslavsky, S. E.; Acuna, A. U.; Adam, W.; Amat, F.; Armesto, D.; Atvars, T. D. Z.; Bard, A.; Bill, E.; Bjoern, L. O.; Bohne, C.; Bolton, J.; Bonneau, R.; Bouas-Laurent, H.; Braun, A. M.; Dale, R.; Dill, K.; Doepp, D.; Duerr, H.; Fox, M. A.; Gandolfi, T.; Grabowski, Z. R.; Griesbeck, A.; Kutateladze, A.; Litter, M.; Lorimer, J.; Mattay, J.; Michl, J.; Miller, R. J. D.; Moggi, L.; Monti, S.; Nonell, S.; Ogilby, P.; Olbrich, G.; Oliveros, E.; Olivucci, M.; Orellana, G.; Prokorenko, V.; Naqvi, K. R.; Rettig, W.; Rizzi, A.; Rossi, R. A.; San, R. E.; Scandola, F.; Schneider, S.; Thulstrup, E. W.; Valeur, B.; Verhoeven,

J.; Warman, J.; Weiss, R.; Wirz, J.; Zachariasse, K. Glossary of Terms Used in Photochemistry, 3rd edition (IUPAC recommendations 2006). *Pure Appl. Chem.* **2007**, *79*, 293-465.
(26) (a) Alfassi, Z. B.; Harriman, A.; Huie, R. E.; Mosseri, S.; Neta, P. The redox potential of the azide/azidyl couple. *J. Phys. Chem.* **1987**, *91*, 2120-2122. (b) Kadija, I. Measurements of the Steady-State Activation Overpotential of Chlorine Evolving Electrodes. *J. Electrochem. Soc.* **1984**, *131*, 601.
(27) Marin, M. L.; Santos-Juanes, L.; Arques, A.; Amat, A. M.; Miranda, M. A. Organic photocatalysts for the oxidation of pollutants and model compounds. *Chem. Rev.* **2012**, *112*, 1710-1750.
(28) Heelis, P. F. The Photophysical and Photochemical Properties of Flavins (Isoalloxazines). *Chem. Soc. Rev.* **1982**, *11*, 15-39.
(29) Larson, R. A.; Stackhouse, P. L.; Crowley, T. O. Riboflavin tetraacetate: a potentially useful photosensitizing agent for the treatment of contaminated waters. *Environ. Sci. Technol.* **1992**, *26*, 1792-1798.